Synergistic effects in the melting of DNA hydration shell: melting of the minor groove hydration spine in poly(dA)·poly(dT) and its effect on base pair stability

Y. Z. Chen and E. W. Prohofsky
Department of Physics, Purdue University, West Lafayette, Indiana 47907 USA

ABSTRACT We propose that water of hydration in contact with the double helix can exist in several states. One state, found in the narrow groove of poly(dA)·poly(dT), should be considered as frozen to the helix, i.e., an integral part of the double helix. We find that this enhanced helix greatly effects the stability of that helix against base separation melting. Most water surrounding the helix is, however, melted or disassociated with respect to being an integral part of helix and plays a much less significant role in stabilizing the helix dynamically, although these water molecules play an important role in stabilizing the helix conformation statically. We study the temperature dependence of the melting of the hydration spine and find that narrow groove nonbonded interactions are necessary to stabilize the spine above room temperature and to show the broad transition observed experimentally. This calculation requires that synergistic effects of nonbonded interactions between DNA and its hydration shell affect the state of water–base atom hydrogen bonds. The attraction of waters into narrow groove tends to retain waters in the groove and compress or strain these hydrogen bonds.

INTRODUCTION

It has been established that water of hydration is essential for DNA double helical stability. Recent x-ray analysis has found that a well-defined hydration spine is present in the minor groove for particular sequences (Kopka et al., 1983; Alexeev et al., 1987; Chuprina, 1987; Larsen et al., 1991; Narayana et al., 1991; Prive et al., 1991; Teplukhin et al., 1992). The occurrence of such specific water locations is, however, not the general case and for the most part the waters of hydration appear not to have specific localizable positions with respect to the double helix. In this paper we explore the proposition that specific hydration spines can exist in the narrow groove, which can be considered bonded to, and an integral part of, the helix over some temperature range. We expect, as proposed by Herrera and Chaires (1989), that this hydrogen-bonded spine can melt or separate from the rest of the helix, much like the strand separation melting studied by many and that we have studied extensively by modified selfconsistent phonon approximation (MSPA) theory. In this paper we apply MSPA theory to explore the melting of the spine of hydration and we find that the calculated melting profile can match the observations of Herrera and Chaires (1989) when one specifically includes nonbonded interactions between helix and spine associated with the narrow groove conformation. Without such an attractive pocket effect, the spine structure melts or separates from the helix below the freezing temperature of water. This result indicates that only in a narrow groove are structured hydration spines possible above 0°C and explains why most water of hydration is not at well-defined positions.

In our earlier studies (Chen et al., 1991*a*, *b*, 1992; Chen and Prohofsky, 1993), which have ignored the explicit role of water of hydration, we have shown that MSPA theory can be used to predict DNA interbase H-bond disruption probabilities and base pair opening probabilities, both in the premelting temperature regime and in the helix–coil transition region. We showed that the disruption of an amino interbase H-bond can be associated with the "open state" needed to facilitate amino proton exchange (Teitelbaum and Englander, 1975; Preisler et al., 1984). This association holds for the two amino H-bonds in a GC base pair as well as the one amino H-bond in an AT base pair. We also showed that a base pair open state, in which all the interbase H-bonds are simultaneously disrupted, can be associated with the "open state" needed to facilitate imino proton exchange (Leroy et al., 1985; Gueron et al., 1987, 1990). Our calculated probabilities are in fair agreement both with proton exchange measurements at premelting temperatures and with the transition profile obtained from the melting measurements.

Because of the difficulties involved in the structural modeling of the hydration shells surrounding DNA, the dynamic coupling between DNA atoms and the water molecules in the hydration shells was explicitly neglected in our earlier calculations, except in the case where a well-organized minor groove hydration spine was considered for poly(dA)·poly(dT) (Chen and Prohofsky, 1992). The agreement with experimental observation of these other earlier calculations, in which no explicit hydration effects were considered, may seem to be surprising. Indeed, the water molecules in the DNA hydration shells play both a static and a dynamic role. The static role of water molecules is important in stabilizing the DNA double helix and in the determination of DNA conformation (Dickerson, 1983; Saenger, 1984; Saenger et al., 1986). Dynamically these water molecules strongly influence DNA vibrations in the frequency range of several to a few hundred gigahertz (Tominaga et

Address correspondence to Dr. Earl W. Prohofsky, Department of Physics, 1396 Physics Building, Purdue University, West Lafayette, IN 47907-1396, USA.

0006-3495/93/05/1385/09 $2.00

al., 1985; Tao and Lindsay, 1987, 1988). The reason that the MSPA calculations can in some cases give reasonable results without explicitly considering the hydration shells is that the static contribution is implicitly included in the lattice dynamic formulation of DNA. In the MSPA formulation, one assumes all the static forces are balanced and a DNA double helix is stabilized at a specific conformation by static forces, part of which is, of course, from the hydration shells. Some of the water dynamic effects are included in our studies by including a proper set of dielectric constants for the coulomb interactions. These take into account the fact that some long-range interactions are mediated by the presence of the water molecules in the hydration shells. Although additional dynamic coupling between DNA and its melted hydration shells is neglected, if included it would only affect normal modes below $\sim 30\ cm^{-1}$ (Tominaga et al., 1985; Tao and Lindsay, 1987, 1988). The most significantly affected modes are at even lower frequencies, which are centered at $16\ cm^{-1}$ for B-form DNA fiber. These modes are away from the frequency range of the soft modes of the interbase H-bonds, which are centered at $\sim 85\ cm^{-1}$ (Urabe et al., 1985; Weidlich and Lindsay, 1988). Therefore one expects that the dynamic coupling between DNA and its melted hydration shells has only a limited effect on the base pair thermal fluctuational stability. We show that this is the case later in this paper.

Our earlier work has shown, however, that the minor groove spine of hydration, when incorporated into the helix as an integral part of the helix, strongly influences the thermal fluctuational stability of the base pairs to which it is attached (Chen and Prohofsky, 1992). This spine of hydration was found to exist in the minor groove of poly(dA)·poly(dT) (Alexeev et al., 1987; Chuprina, 1987; Teplukhin et al., 1992) as well as in the central region of several B-DNA dodecamers (Kopka et al., 1983; Larsen et al., 1991; Narayana et al., 1991; Prive et al., 1991). This spine is composed of two layers of water molecules. The first layer consists of one water molecule per base pair. That water molecule forms a H-bond to an adenine N_3 atom in one base pair and it forms another H-bond to the thymine O_2 atom in the adjacent base pair. The second layer also consists of one water molecule per base pair. That water molecule bridges between the two neighboring first-layer water molecules. Recent simulation studies (Chuprina et al., 1991; Teplukhin et al., 1992) revealed that the existence of such a spine depends predominantly on the DNA groove width. Our own study[1] showed that for a spine model with a realistic H-bond potential a strong pocket attraction is necessary for the stabilization of the spine at physiological temperatures. This is in agreement with the conclusion from simulations.

[1] Y. Z. Chen and E. W., Prohofsky, manuscript submitted for publication.

In this paper we present results from four calculations using varying models for spine–helix interactions. One calculation explores the melting and premelting base pair stability for poly(dA)·poly(dT) with no explicit hydration coupling. This model analysis is included to show how the helix would behave in the absence of a bound hydration spine. It can be thought of as a baseline for interpreting the effects that arise from incorporating the hydration spine. In case 2 we introduce the narrow groove spine described above, and the spine interacts with the helix both by nonbonded Van der Waals and electrostatic interactions as well as by H-bonds to the bases as described above. The H-bond strength is that expected for the atoms and distances involved. This model is included to show that the simple inclusion of a hydration spine without incorporating the synergistic effects described below does not lead to calculated behavior that is in agreement with the observations. In fact, this simple spine model does not increase the helix melting temperature; the spine has itself melted below the helix melting temperature. This model does, however, illustrate the limited role of water that is present in the vicinity of the helix and in the melted form, on the dynamic stability of the helix, although these waters play an important role in stabilizing the helix conformation statically.

The third case is very much like the second case, except that the strength of the spine water–base atom H-bond interaction is increased to a level that increases the helix stability so that poly(dA)·poly(dT) melts at the observed melting temperature. This model is included to show that simply increasing the strength of the spine bonding to the helix is, again, not sufficient to show the melting behavior observed. Although this approximation can increase the melting temperature of the helix to the observed values, it does not display the broad premelting increase in base unstacking that is observed. This comparison to our case 4 model shows that the synergistic interaction is specifically what is needed to show both the increased melting temperatures and the broad premelting features. Case 4 is again like case 2 in that a reasonable H-bond interaction and nonbonded interactions between helix and spine are included. In addition, we add the synergistic effect of the strong nonbonded interactions on the behavior of the H-bond. This case does show all the features observed, both the anomalous increase in melting temperature as well as the premelting feature. Comparing this case with case 1 does show that hydration spine effects are necessary to achieve the observed melting temperature. Comparison to case 2 shows that simply adding a hydration spine without the synergistic interaction does not raise the melting temperature and does not show the premelting feature. Comparison to case 3 shows that even artificially increasing the coupling between the spine and helix does not show the premelting feature, even though it can, of course, be made to fit the observed melting temperature.

Our case 4 model does show both the anomalous increase in melting temperature and the premelting feature, and we argue that a model must contain the synergistic effects we incorporate into it to show both. We believe case 4 to be our best model for helix melting in the presence of a spine of hydration.

This synergistic effect is one we have explored in an earlier work to explain the stability of the helix in the presence of coulomb repulsion. In that work the coulomb forces introduce a tensile stress that tends to pull the interbase H-bonds apart (Chen et al., 1992).[1] The stress caused a strained H-bond that generated the compensating stress that kept the system stable. That work, by including the effect of stress on the H-bond, led to a theory of the melting temperature of poly(dG)·poly(dC) as a function of salt concentration, in fair agreement with observations. In the current problem, in which the nonbonded forces attract the waters into a narrow groove, the stress on the H-bonds is reactive. The pocket attraction actually compresses the water–base atom H-bonds compared with what they would be in the absence of the compression. It is this synergistic effect of pocket and H-bond that is essential to get the broadened spine dissociation transition in agreement with the observations of Herrera and Chaires (1989).

We have also studied the effect of compression of the interbase H-bonds by hydrostatic pressure.[1] We have applied the same concept of compression-strained bonds in that calculation. The hydrostatic pressure compresses the entire helix and the compression is necessarily also effected across the interbase H-bonds. Only with this synergistic effect of compression were we able to match the experimentally observed pressure dependence of melting of both poly[d(A-T)] and poly(dG)·poly(dC).

We use MSPA methods to be able to use simple statistical estimates of bond fluctuations. Such estimates are not otherwise possible for a system with bounded interatomic potentials, as the statistical equilibrium for such systems is always the evaporated or sublimated state in the absence of a vapor pressure or some form of phase space limitation. In MSPA one has effective unbounded potentials that are determined at each temperature from the true bounded potentials. In practice, then, in MSPA one uses force constants as representative of effective potentials. In the process one loses data that would be available to determine static equilibrium positions from the potentials. The strained bond concept is a way of incorporating the static force effect back into the MSPA theory. MSPA then leads efficiently to calculations that show melting. Use of the entire true potentials would require simulations for solutions and these cannot, as of yet, be run long enough to see melting for DNA, as the time scale for base separation is milliseconds (Gueron et al., 1990).

FORMALISM

As in our earlier studies, the coordinates of poly(dA)·poly(dT) are obtained from the fiber studies of Arnott and Selsing (1974). The spine structure is constructed based on the configuration given by Kopka et al. (1983). The eigenvalues and eigenvectors of the system are obtained from the secular equation

$$(\Phi - \omega^2 \mathbf{I})\mathbf{q} = 0, \qquad (1)$$

where Φ is the force constant matrix, i.e., the matrix of temperature dependent spring constants. The determination of these spring constants will be discussed later. ω and $\mathbf{q}$ are the eigenvalues and eigenvectors in mass-weighted Cartesian coordinates. It is useful to exploit the helical symmetry inherent in the system to reduce the calculation. We divide poly(dA)·poly(dT) into unit cells, each containing one base pair and the associated section of backbones. The secular equation is, therefore, reduced to a number of equations, each of dimensionality of a single cell. The unit cell dimensionality of poly(dA)·poly(dT) with no water molecules attached is 123 × 123. The unit cell dimensionality of poly(dA)·poly(dT) with the minor groove spine of hydration or with the model minor groove hydration shell as integral part of the helix becomes 129 × 129.

To further simplify the calculation, we have assumed the valence force constants and the nonbonded force constants (other than the nearest neighbor base stacking force constants) to be independent of temperature. These force constants are fitted with experimental observations at room temperature. The valence force constants for the bases are from Tsuboi and Takahashi (1983). The refined valence force constants of the backbones can be found in an earlier paper (Lu et al., 1977). The long-range nonbonded force constants are formulated by Devi Prasad and Prohofsky (1984) and the room temperature Van der Waals base stacking force constants are formulated by Young et al. (1989). The base stacking force constants are assumed to have the same temperature dependence as the average value of the interbase H-bonds. The force constants of the intact interbase H-bonds and the force constants of the intact H-bonds in the spine of hydration at room temperature are determined by the Lippincott–Schroeder model (Schroeder and Lippincott, 1957). The spine angle bending valence force constants are obtained by taking the average of the stretch force constants of the bonds involved and then dividing by seven.

To obtain the force constants of the interbase H-bonds and the water-base H-bonds at a different temperature, we model each H-bond by a Morse potential well V_{Morse}, where:

$$V_{\text{Morse}} = V_0\{1 - \exp[-a(R - R_0)]\}^2 - V^0 \qquad (2)$$

Here R is the instantaneous bond length and a, V_0, and R_0 are the Morse parameters. The determination of these

TABLE 1 **Key parameters of the H-bonds**

System	Bond	a	r_0	V_0	L^{max}
		$Å^{-1}$	$Å$	*kcal/mol*	$Å$
AT base pair (all cases)	$N_6—H—O_4$	1.961	2.738	3.543	3.191
	$N_1—H—N_3$	1.909	2.789	3.269	3.119
Spine of hydration (cases 2 and 4)	$N_3—W$	2.316	2.731	2.405	3.004
	$O_2—W$	2.005	2.799	2.362	2.999
Spine of hydration (case 3)	$N_3—W$	2.316	2.634	3.538	3.018
	$O_2—W$	2.004	2.768	3.195	2.999

Parameters determined by cooperative formalism. a, r_0, and V_0 are the Morse parameters and L^{max} is the maximum stretch length.

parameters with cooperative effects of open bonds being considered is described in our earlier work.[1] These parameters are given in Table 1. The force constant of an intact H-bond is obtained as a weighted average over stretches:

$$\phi_i^{int} = A_i \int_{-h_i}^{\infty} du e^{-u^2/2D_i} \frac{d^2}{du^2} V_{Morse}(R_i + u), \quad (3)$$

where A_i is a normalization factor,

$$A_i^{-1} = \int_{-h_i}^{\infty} du e^{-u^2/2D_i}, \quad (4)$$

and $-h_i$ is the hard-core inner boundary. D_i is the mean square stretching amplitude of the H-bond,

$$D_i = \frac{1}{\pi} \sum_{\lambda} \int_0^{\pi} d\theta \frac{|s_i^{\lambda}(\theta)|^2}{2\omega_{\lambda}(\theta)} \coth\left[\frac{\omega_{\lambda}(\theta)}{2k_B T}\right], \quad (5)$$

where s_i is a projection on the internal stretch coordinate of the H-bond normal mode eigenvector. When the cooperative effects associated with disrupted bonds and open base pairs are taken into consideration, the H-bond force constant ϕ_i and the nearest neighbor cross-strand stacking force constant ϕ_s can be given by:

$$\phi_i = (1 - P_i)\phi_i^{int}$$
$$\phi_s = (1 - P_{op})\phi_s^{int}. \quad (6)$$

P_i is the individual bond disruption probability,

$$P_i = A_i \int_{L_i^{max}}^{\infty} du \exp[-(u - R_i)^2/2D_i], \quad (7)$$

and L_i^{max} is the maximum bond stretch length before disruption (Chen and Prohofsky, 1991). The value of L_i^{max} for each of the H-bonds is given in Table 1. P_{op} is the base pair opening probability. For a base pair with no spine it is given by (Chen and Prohofsky, 1991)

$$P_{op} = \prod_{\text{interbase-H-bonds}} P_i. \quad (8)$$

For a base pair that has the spine, both interbase and spine H-bonds must be disrupted, and it is given by (Chen and Prohofsky, 1992)

$$P_{op} = P_{sp} \prod_{\text{interbase-H-bonds}} P_i$$
$$P_{sp} = (P_{W-N3} + P_{W-O2} - P_{W-N3} \times P_{W-O2}). \quad (9)$$

Finally, the mean length of an interbase H-bond is given, as a probability-weighted linear combination of intact bond length and open bond end atom distance, by

$$R_i = (1 - P_{op})R_i^{int} + P_{op}(L_i^{max} + 2P_i\sqrt{2D_i}). \quad (10)$$

Similarly, the mean length of a spine water–base atom H-bond is given by

$$R_i^{sp} = (1 - P_{sp})(R_i^{int} + dr_i^{sp}) + P_{sp}(L_i^{max} + 2P_i\sqrt{2D_i}), \quad (11)$$

where R_i^{int} is the mean thermally expanded length of an intact bond determined by the condition $V_i(R_i^{int} + \mu_i) = V_i(R_i^{int} - \mu_i)$. $\mu_i = 2\sqrt{2D_i \ln 2}$ is the full width at half-maximum of the vibrational distribution function.

dr_i^{sp} is the synergistically induced strain to the spine water–base atom H-bond from the pocket attraction of the atoms on the surface of the minor groove.[1] The nonbonded Van der Waals forces acting between the DNA and the spine water molecules create a tension that is expressed across the two intervening water–base atom H-bonds. This tension, in turn, generates a compensating stress that arises from an induced strain or change in the mean bond length of the intervening H-bond. These forces have to be balanced to give a stable DNA + spine structure.

The compensating stress of a water–base atom H-bond $f_i^h(R_i)$ and the static force from the Van der Waals pocket attraction $\mathbf{f}^{VW}$ can be calculated from the relevant potentials:

$$f_i^h(R_i) = -\frac{dV_{Morse}(R_i)}{dR_i}$$
$$\mathbf{f}^{VW} = -\sum \nabla V_{VW}(R). \quad (12)$$

The Van der Waals parameters are calculated by using the Slater–Kirkwood formula. The Slater–Kirkwood parameters for the base atoms are from Gelin and Karplus (1979), and the Slater–Kirkwood parameters for a water molecule are extrapolated from the water–water potential energy fitted to the equilibrium dimer properties

(Perez et al., 1983). The force $\mathbf{f}^{VW}$ can be rewritten as the vector summation of the individual forces along the water–base atom H-bond orientation. Let us assume the unstrained mean length of the ith water–base H-bond as determined above is $R_i^{int}(T_0)$. Here T_0 is room temperature. This length will be changed to $R_i^{int}(T_0) + dr_i^{sp}$ when the DNA–spine Van der Waals interactions are present. The condition of balance of force implies that

$$f_i^h[R_i^{int}(T_0) + dr_i^{sp}] - f_i^h[R_i^{int}(T_0)] + f_i^{VW} = 0. \quad (13)$$

By substituting the Morse potential (Eq. 2) into this equation, one obtains

$$dr_i^{sp} = \frac{1}{a} \ln \frac{\eta_i}{1 + \sqrt{(\eta_i - 1)^2 - 2f_i^{VW}/aV_0}}, \quad (14)$$

where $\eta_i = 2\exp[-a(R_i^{int}(T_0) - r_0)]$, f_i^{VW} is the component of the pocket attractive force in the ith water–base atom H-bond orientation, and a, r_0, and V_0 are the Morse parameters. dr_i^{sp} is zero for cases 1–3 and is used only in the case 4 calculation. This strain is incorporated into the effective force constant calculation by including it in determining the centroid of weighting function in Eq. 3.

By solving Eq. 1 one obtains the normal mode eigenfrequencies and eigenvectors of the system. These eigenfrequencies and eigenvectors can then be used to calculate vibrational amplitudes, bond lengths, and bond disruption probabilities, etc. These, in turn, are used to redefine the effective force constants. This process continues until the system reaches self-consistency at a given temperature (Gao et al., 1984; Chen et al., 1990; Chen and Prohofsky, 1991).

At temperatures where the spine is stable, the position of a first-layer water molecule is determined from the calculated water–base atom distances. At temperatures where the spine is disrupted, we determine the position of that water molecule by using the realistic end atom distances of the locally disrupted spine given in our earlier calculation.[1] Our calculations show that a water–water H-bond force constant is significantly larger than a water–base atom H-bond force constant (Chen and Prohofsky, 1992).[1] This indicates that the bonding between a first-layer water molecule and a second-layer water molecule is much stronger than the bonding between a base atom and a first-layer water molecule. We therefore assume the H-bond between a first-layer water molecule and a second-layer water molecule remains intact in the whole temperature range considered in this study. The parameters used in our numerical calculations for the various cases are listed in Table 1. The parameters are determined using the fixed bond length, force constant, and dissociation energy. In this study we take into account the effects associated with the open base pairs and disrupted bonds. Therefore, these parameters are slightly different from that of noncooperative formulation.

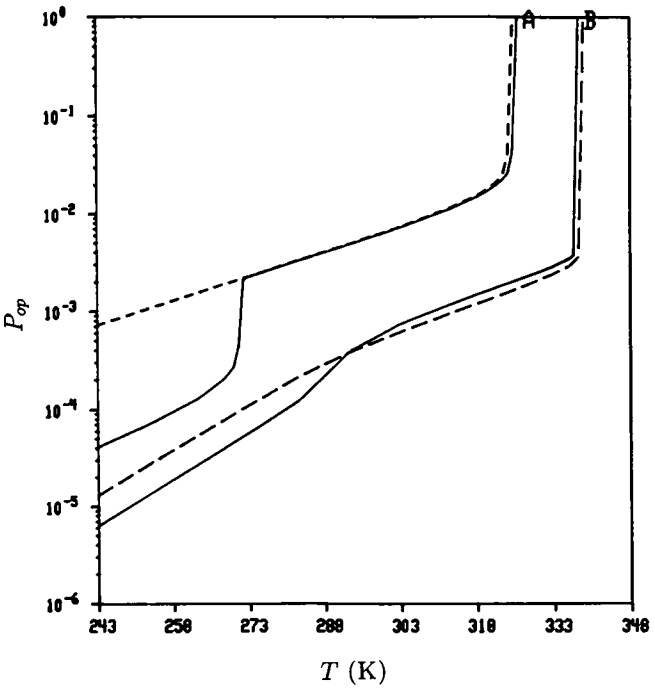

FIGURE 1 Calculated base pair opening probability P_{op} of poly(dA)·poly(dT) as a function of temperature. The lines are arranged as follows: short dashed line is for case 1, solid line A is for case 2, long dashed line is for case 3, and solid line B is for case 4.

RESULTS AND DISCUSSION

The case 1 calculation is the simplest and is similar to many of our earlier calculations that have ignored explicit roles for the water of hydration. The P_{op} for the two interbase H-bonds of this polymer is shown as a function of temperature in Fig. 1 (*short dashed line*). The rapid increase in P_{op} at 326°K indicates cooperative melting sets in at this temperature for this model. This is well below the observed melting temperature of poly(dA)·poly(dT) for these salt concentrations (~0.05 M NaCl).

The case 2 calculation for P_{op} is also shown Fig. 1 (solid line A). The rapid increase in P_{op} at 272°K is associated with a cooperative melting of the spine helix H-bonds, which leaves the interbase H-bonds mostly still intact. The greater rise in P_{op} at 327°K is the cooperative melting of interbase H-bonds and hence the melting of the helix. Note that over the range from 272 to 326°K, P_{op} for the case 2 calculation is very close to that of the case 1 calculation. This is so even though nonbonded interactions between the spine waters and atoms of the helix are taking place in the case 2 calculation. This interaction does stabilize the helix by a trivial amount; raising the melting temperature by 1°K (from 326 to 327°K). The effect of the melted spine above 272°K is insignificant. A melted spine of hydration has little effect on the melting dynamics. This calculation, using realistic values for all parameters in the system, is clearly incor-

TABLE 2 **Premelting base pair P_{op} and the P_{Aam} of poly(dA)·poly(dT)**

	P_{Aam}				P_{op}			
T	Case 1	Case 2	Case 3	Case 4	Case 1	Case 2	Case 3	Case 4
°K		$\times 10^{-2}$				$\times 10^{-3}$		
243	1.44	1.30	1.27	1.26	0.72	0.04	0.01	0.006
253	1.85	1.65	1.62	1.60	1.07	0.07	0.03	0.01
263	2.37	2.10	2.06	2.03	1.57	0.13	0.05	0.03
273	3.01	2.99	2.59	2.56	2.29	2.27	0.11	0.06
283	3.85	3.81	3.25	3.20	3.34	3.30	0.22	0.13
293	5.94	4.89	4.03	4.04	4.91	4.83	0.38	0.39
303	6.44	6.35	5.00	5.03	7.34	7.18	0.62	0.74
313	8.75	8.57	6.25	6.33	11.6	11.3	0.96	1.18
323	14.7	13.7	7.86	7.96	24.9	22.4	1.49	1.86
333			10.0	10.1			2.42	2.91

T, temperature; P_{Aam}, Adenine amino interbase H-bond disruption probability; P_{op}, opening probability.

rect, as it predicts a wrong melting temperature for the helix as well as no broad premelting transition.

The case 3 calculation is shown in Fig. 1 (*long dashed line*). This calculation has an unrealistically strong H-bond coupling, which was chosen so as to have the helix melting temperature fit the observed melting temperature. The calculation does not show the broad premelting transition observed by Herrera and Chaires (1989) and is thus also in disagreement with observation.

The case 4 calculation, which has reasonable parameters for all the H-bonds and includes the effect of pocket attracting strain on the water–base H-bonds, is in Fig. 1 (solid line *B*). The result has all the features seen by Herrera and Chaires (1989) in their study of poly(dA)·poly(dT) melting; in particular, it shows the broad premelting transition. The study of Herrera and Chaires (1989) measures the ultraviolet (UV) absorption change at premelting temperatures. The UV absorption intensity depends strongly on the status of base stacking. Hence, there should be a correspondence between the UV curve and base pair opening probability. However, the comparison between our calculation and Herrera and Chaires's measurement is not straightforward, since the measurement was carried out at a different salt concentration than our nominal salt concentration. In Table 2 we list the premelting individual H-bond disruption probability (from Eq. 7) as a function of temperature for our most realistic model (case 4) and, for comparison, that for the other models. P_{Aam} would describe the open state probability associated with amino proton exchange. P_{op} would be the open state associated with imino proton exchange. The spine has a greater stabilizing effect at lower temperatures, which is reduced at higher temperatures as the spine has higher probability of itself being disassociated.

In Fig. 2 we concentrate on the melting of the hydration spine attachment to the helix rather than the melting of the helix itself. The probability that at least one of the H-bonds between the spine and helix are open, P_{sp}, is plotted as a function of temperature for cases 2–4. Case 1 has no spine to melt. The rapid rise in P_{sp} at 272°K in case 2 shows a cooperative melting that occurs below the freezing temperature of water. This is not surprising, inasmuch as the H-bonds between the spine and helix are weaker than the H-bonds between water itself. Water H-bonds should remain intact to higher temperatures than the H-bonds between water and helix. The case 3 P_{sp}, shown as the dashed line, is frozen to the helix until the helix itself melts. This is due to the unreasonably strong H-bonding between spine and helix of this model. It should be noted that both cases 2 and 3 show a sharp cooperative melting. An intermediate strength H-bond would show a cooperative helix spine melt at an intermediate temperature. No unstrained model system, regard-

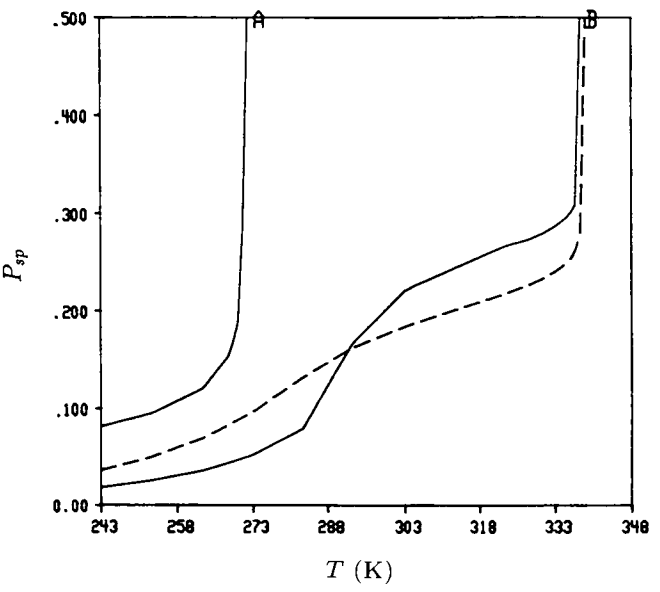

FIGURE 2 Calculated spine disruption probability P_{sp} as a function of temperature. The solid line *A* is for case 2, the long dashed line is for case 3, and the solid line *B* is for case 4.

TABLE 3 Calculated P_{sp} and bond disruption probabilities of the water-base atom H-bonds of our spine models in poly(dA)·poly(dT)

	P_{N_3-W}			P_{O_2-W}			P_{sp}		
T	Case 2	Case 3	Case 4	Case 2	Case 3	Case 4	Case 2	Case 3	Case 4
°K		$\times 10^{-1}$			$\times 10^{-1}$			$\times 10^{-1}$	
243	0.53	0.25	0.10	0.30	0.12	0.09	0.82	0.37	0.19
253	0.62	0.35	0.14	0.35	0.16	0.12	0.95	0.51	0.26
263	0.81	0.49	0.21	0.43	0.21	0.16	1.21	0.70	0.37
273		0.70	0.32		0.29	0.21		0.97	0.53
283		0.96	0.51		0.40	0.30		1.31	0.79
293		1.18	1.19		0.50	0.54		1.62	1.67
303		1.33	1.56		0.58	0.76		1.83	2.21
313		1.45	1.67		0.65	0.93		2.00	2.44
323		1.58	1.75		0.70	1.10		2.17	2.66
333		1.79	1.81		0.74	1.29		2.40	2.87

T, temperature; P_{sp}, premelting spine disruption probability; P_{N_3-W} and P_{O_2-W}, bond disruption probabilities.

less of H-bond strength, has shown the kind of broad melting transition that is shown by the case 4 calculation.

The case 4 calculation, with an H-bond strained by nonbonded attractions to the narrow groove, is shown as the lower solid line in Fig. 2. The breakup of the H-bonds between waters and helix, which would otherwise look like that in case 2, is retarded by the synergistic strain effects. The capture into the pocket of the spine retards the melting transition. The melting of the spine is still incomplete above 330°K, when cooperative melting of the helix occurs and destroys the narrow groove pocket. At this point melting of the spine proceeds to completion.

The difference between our case 2 and 4 studies, shown in Fig. 2, shows that the sizable strain on the spine–helix H-bonds greatly stabilizes the attachment of the spine to the helix. The close proximity to the spine of the many atoms on the surface of the narrow groove gives rise to the attraction that causes this strain. In a wider groove this attraction would be reduced, as fewer atoms could simultaneously be that close to the waters of the spine. The individual H-bonding, however, can be to a single site and may be comparable in strength to our model H-bond at several locations. One would expect that models for other possible hydration chains would, therefore, give results on chain attachment somewhere between what we find for our case 2 and 4 calculations but likely closer to our case 2 calculations. We expect that such a possible spine would melt at any location other than in the narrow groove. We expect most water of hydration not in a narrow groove to be melted and only weakly dynamically coupled to the helix. In Table 3 we list the individual and combined bond disruption probabilities for cases 2–4 as a function of temperature.

In Fig. 3 we show the temperature dependence of the spine H-bond force constants for cases 2–4. The temperature dependence of the force constants in case 3 has features similar to the force constants in case 2. This is expected, as the third case is very much like the second case except that the strength of the interaction in case 3 is increased. We find that the introduction of a stress-induced strain in the spine H-bonds significantly alters the temperature-dependent behavior of the force constants. The force-constant curves of case 4 all show a typical synoidal form. It is this feature that determines the particular temperature dependence of the open probabilities of the case 4 calculations as shown in Figs. 1 and 2. In contrast to the spine H-bond force constants, the differences between the interbase H-bond force constants in

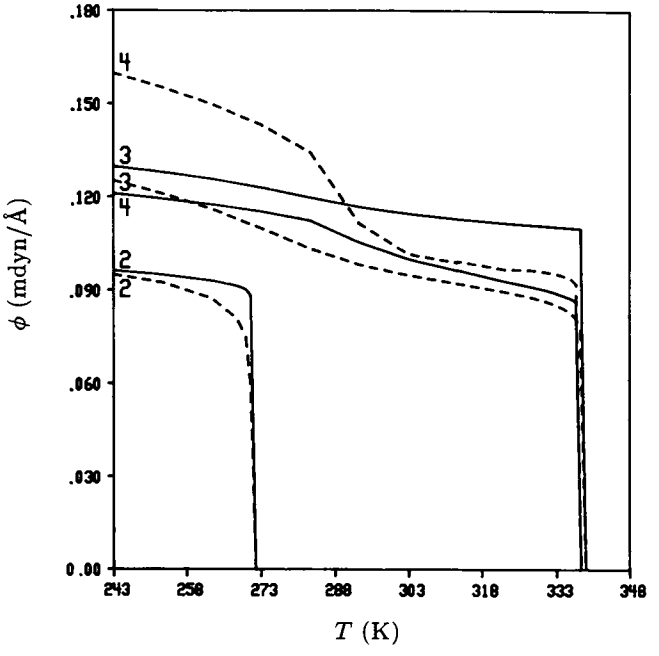

FIGURE 3 Calculated force constants of the spine H-bonds as a function of temperature. The solid lines are for the O_2-W bond and the dashed lines are for the N_3-W bond. The numbers near the lines indicate the case number. These force constants are in units of mdyn/Å (1 mdyn = 10^{-8} newton).

TABLE 4 **Force constants of the interbase H-bonds of poly(dA)·poly(dT) at several premelting temperatures**

	$\phi_{N_6-H-O_4}$				$\phi_{N_1-H-N_3}$			
T	Case 1	Case 2	Case 3	Case 4	Case 1	Case 2	Case 3	Case 4
°K	*mdyn/Å*				*mdyn/Å*			
243	0.125	0.126	0.127	0.127	0.116	0.120	0.122	0.123
253	0.122	0.123	0.124	0.124	0.113	0.118	0.120	0.121
263	0.118	0.120	0.120	0.121	0.111	0.116	0.118	0.119
273	0.114	0.114	0.117	0.117	0.108	0.108	0.116	0.116
283	0.110	0.110	0.113	0.113	0.104	0.104	0.113	0.114
293	0.104	0.105	0.109	0.109	0.101	0.101	0.111	0.111
303	0.098	0.098	0.105	0.105	0.097	0.097	0.108	0.108
313	0.089	0.090	0.100	0.099	0.092	0.092	0.105	0.105
323	0.071	0.074	0.094	0.093	0.082	0.084	0.102	0.102
333	0.0	0.0	0.087	0.086	0.0	0.0	0.098	0.098

T, temperature; ϕ, force constant for indicated bonds.

different case calculations are less obvious. In Table 4 we give the force constants of the individual interbase H-bonds for all the cases at several premelting temperatures. We find that, in general, the differences between cases 1 and 2 and the differences between cases 3 and 4 are marginal. Another feature is that the force constant of the bond closer to the spine (N1−H−N3 bond) has a higher sensitivity to the minor groove hydration status than that of the bond in the major groove (N6−H−O4 bond).

At very low temperature all our model spines are stable. This seems to indicate that a well-organized hydration network may be able to form in a wider groove, where pocket attraction is weaker than that of a narrow minor groove, at very low temperatures. It would be interesting to see whether some kind of spine structure can be observed in those DNA sequences with a wider minor groove at low temperature. As shown in Table 3, the calculated spine disruption probability P_{sp} is ~20% at 270°K and ~10% at 253°K. P_{sp} further decreases as the temperature is lowered further. The likelihood of observation of some kind of spine structure should be high at very low temperatures. Recent low-temperature crystal structural analysis of Narayana et al. (1991) on a B-DNA oligomer, CGTGAATTCACG, does seem to indicate the existence of a spine structure in a wider minor groove at very low temperatures. Narayana et al. (1991) observed that at 183°K there are water molecules beyond the spine observed by Kopka et al. (1983) at higher temperatures. These water molecules extend into the end part of the duplex and they are involved in the minor groove interactions not seen before.

This work is supported in part by Office of Naval Research contract N00014-92-K-1232.

Received for publication 18 September 1992 and in final form 7 December 1992.

REFERENCES

Alexeev, D. G., A. A. Lipanov, and I. Y. Skuratovskii. 1987. Poly(dA)·Poly(dT) is a B-type double helix with a distinctively narrow minor groove. *Nature (Lond.)*. 325:821–823.

Arnott, S., and E. Selsing. 1974. Structures for the polynucleotide complexes Poly(dA)·Poly(dT) and Poly(dA)·Poly(dA)·Poly(dT). *J. Mol. Biol.* 88:509–523.

Chen, Y. Z., and E. W. Prohofsky. 1991. A self-consistent mean-field calculation of a homopolymer deoxyribose nucleic acid strand separation: bond breaking in a macromolecule. *J. Chem. Phys.* 94:4665–4667.

Chen, Y. Z., and E. W. Prohofsky. 1992. The role of a minor groove spine of hydration in stabilizing Poly(dA)·Poly(dT) against fluctuational interbase H-bond disruption in the premelting temperature regime. *Nucleic Acids Res.* 20:415–419.

Chen, Y. Z., and E. W. Prohofsky. 1993. A cooperative self-consistent microscopic theory of thermally induced melting of a repeat sequence DNA polymer. *Biopolymers.* 33:351–362.

Chen, Y. Z., Y. Feng, and E. W. Prohofsky. 1990. Criterion of thermal denaturation for modified-self-consistent-phonon-theory mean-field calculations in DNA polymers. *Phys. Rev.* B42:11335–11338.

Chen, Y. Z., Y. Feng, and E. W. Prohofsky. 1991*a*. Premelting thermal fluctuational base pair opening probability of Poly(dA)·Poly(dT) as predicted by the modified self-consistent phonon theory. *Biopolymers.* 31:139–148.

Chen, Y. Z., W. Zhuang, and E. W. Prohofsky. 1991*b*. Premelting thermal fluctuational interbase hydrogen-bond disrupted states of a B-DNA guanine-cytosine base pair: significance for amino and imino proton exchange. *Biopolymers.* 31:1273–1281.

Chen, Y. Z., W. Zhuang, and E. W. Prohofsky. 1992. Salt-dependent stability of Poly(dG)·Poly(dC) with potential of mean force coulomb interactions. *Biopolymers.* 32:1123–1127.

Chuprina, V. P. 1987. Anomalous structure and properties of Poly(dA)·Poly(dT). Computer simulation of the polynucleotide structure with the spine of hydration in the minor groove. *Nucleic Acids Res.* 15:293–311.

Chuprina, V. P., U. Heinemann, A. A. Nurislamov, P. Zielenkiewicz, and R. E. Dickerson. 1991. Molecular dynamics simulation of the hydration shell of a B-DNA decamer reveals two main types of minor-groove hydration depending on groove width. *Proc. Natl. Acad. Sci. USA.* 88:593–597.

Devi Prasad, K. V., and E. W. Prohofsky. 1984. Low-frequency lattice mode predictions in A-DNA compared to experimental observa-

tions and significance for A-to-B conformation change. *Biopolymers.* 23:1795–1798.

Dickerson, R. E. 1983. The DNA helix and how it is read. *Sci. Am.* 249:94–110.

Gao, Y., K. V. Devi-Prasad, and E. W. Prohofsky. 1984. A self-consistent microscopic theory of hydrogen bond melting with application to Poly(dG)·Poly(dC). *J. Chem. Phys.* 80:6291–6298.

Gelin, B. R., and M. Karplus. 1979. Side-chain torsional potentials: effect of dipeptide, protein and solvent environment. *Biochemistry.* 18:1256–1260.

Gueron, M., M. Kochoyan, and J. L. Leroy. 1987. A single mode of DNA base-pair opening drives imino proton exchange. *Nature (Lond.).* 328:89–92.

Gueron, M., E. Charretier, J. Hagerhorst, M. Kochoyan, J. L. Leroy, and A. Moraillon. 1990. Application of imino proton exchange to nucleic acid kinetics and structures. *In Structure & Methods.* DNA & RNA. Vol. 3. R. H. Sarma and M. H. Sarma, editors. Adenine Press, New York. 113–137.

Herrera, J. E., and J. B. Chaires. 1989. A premelting conformational transition in Poly(dA)·Poly(dT) coupled to daunomycin binding. *Biochemistry.* 29:1993–2000.

Kopka, M. L., A. V. Fratini, H. R. Drew, and R. E. Dickerson. 1983. Ordered water structure around a B-DNA dodecamer. A quantitative study. *J. Mol. Biol.* 163:129–146.

Larsen, T. A., M. L. Kopka, and R. E. Dickerson. 1991. Crystal structure analysis of the B-DNA dodecamer CGTGAATTCACG. *Biochemistry.* 30:4443–4449.

Leroy, J. L., D. Broseta, and M. Gueron. 1985. Proton exchange and base-pair kinetics of Poly(rA)·Poly(rU) and Poly(rI)·Poly(rC). *J. Mol. Biol.* 184:165–178.

Lu, K. C., E. W. Prohofsky, and L. L. Van Zandt. 1977. Vibrational modes of A-DNA, B-DNA, and A-RNA backbones: an application of a Green-function refinement procedure. *Biopolymers.* 16:2491–2506.

Narayana, N., S. Ginell, I. M. Russu, and H. M. Berman. 1991. Crystal and molecular structure of a DNA fragment: d(CGTGAATTCACG). *Biochemistry.* 30:4449–4455.

Perez, P., W. K. Lee, and E. W. Prohofsky. 1984. Study of hydration of the Na^+ ion using a polarizable water model. *J. Chem. Phys.* 79:388–392.

Preisler, R. S., C. Mandal, S. W. Englander, and N. R. Kallenbach. 1984. Premelting and the hydrogen-exchange open state in synthetic RNA duplexes. *Biopolymers.* 23:2099–2125.

Prive, G. G., K. Yanagi, and R. E. Dickerson. 1991. Structure of the B-DNA Decamer C-C-A-A-C-G-T-T-G-G and comparison with isomorphous decamers C-C-A-A-G-A-T-T-G-G and C-C-A-G-G-C-C-T-G-G. *J. Mol. Biol.* 217:177–199.

Saenger, W. 1983. *Principles of Nucleic Acid Structure.* Springer-Verlag, New York. 1984. 368–384.

Saenger, W., W. N. Hunter, and O. Kennard. 1986. DNA conformation is determined by economics in the hydration of phosphate groups. *Nature (Lond.).* 324:385–388.

Schroeder, R., and E. Lippincott. 1957. Potential function model of hydrogen bonds. II. *J. Phys. Chem.* 61:921–928.

Tao, N. J., and S. M. Lindsay. 1987. The dynamics of the DNA hydration shell at gigahertz frequencies. *Biopolymers.* 26:171–188.

Tao, N. J., and S. M. Lindsay. 1988. Dynamic coupling between DNA and its primary hydration shell studied by Brillouin scattering. *Biopolymers.* 27:1655–1671.

Teitelbaum, H., and S. W. Englander. 1975. Open state in native polynucleotides. II. Hydrogen-exchange study of Cytosine-containing double helices. *J. Mol. Biol.* 92:79–92.

Teplukhin, A. V., V. I. Poltev, and V. P. Chuprina. 1992. Dependence of the hydration shell structure in the minor groove of the DNA double helix on the groove width as revealed by Monte Carlo simulation. *Biopolymers.* 32:1445–1453.

Tominaga, Y., M. Shida, K. Kubota, H. Urabe, Y. Nashimura, and M. Tsuboi. 1985. Coupled dynamics between DNA double helix and hydrated water by low frequency Raman spectroscopy. *J. Chem. Phys.* 83:5972–5975.

Tsuboi, M., and S. Takahashi. 1973. Infrared and Raman spectra of nucleic acids—vibrations in the base-residues. *In Physico-Chemical Properties of Nucleic Acids.* J. Duchesne, editor. Vol. 2. Academic Press, New York. 91–145.

Urabe, H., H. Hayashi, Y. Tominaga, K. Kubota, and M. Tsuboi. 1985. Collective vibrational modes in molecular assembly of DNA and its application to biological systems. Low frequency Raman spectroscopy. *J. Chem. Phys.* 82:531–535.

Weidlich, T., and S. M. Lindsay. 1988. Raman study of the low-frequency vibrations of polynucleotides. *J. Phys. Chem.* 92:6479–6482.

Young, L., V. V. Prabhu, and E. W. Prohofsky. 1989. Calculation of far-infrared absorption in polymer DNA. *Phys. Rev.* A39:3173–3180.